Simulation

Applications

Simulation: Transactions of the Society for Modeling and Simulation International
1–13

DOI: 10.1177/0037549718802894
journals.sagepub.com/home/sim
SAGE SCS

Finite difference method for solving crack problems in a functionally graded material

A Dorogoy

Abstract

A linear elastic two-dimensional formulation for functionally graded materials is presented. The two-dimensional equilibrium equations and boundary conditions in an orthogonal curvilinear coordinate system are written explicitly. The finite difference technique is used to solve the above formulation. The solution technique is verified by solving two test problems, in which the material is graded horizontally and vertically. The results are compared to analytical results and have very good agreement. The solution technique is then applied to solve a long layer containing an edge crack in which it is assumed that the Young's modulus varies continuously along its width. The problem is solved for two loading conditions: tension and bending. The mode I stress intensity factor is extracted by applying three methods: *J* line and two versions of a modified conservative *J* integral for graded materials. All three methods provide similar results, which are in excellent agreement with the semi-analytical results in the literature. These results demonstrate the applicability of the finite difference technique for solving crack problems in functionally graded materials.

Keywords

Functionally graded materials, finite difference method, edge crack, stress intensity factor

1. Introduction

The development of functionally graded materials (FGMs) offers new alternatives for engineering design. These materials enable engineers to tailor the material properties of a part, and not just its dimensions or shape, to meet design objectives and constraints. FGMs are characterized by gradual spatial changes in their properties due to changes in their composition or structure. Usually, they are composites, but they can also be monolithic materials that do not contain well-defined boundaries or interfaces between their various regions.[1] The smooth transition of properties avoids high interlaminar stresses and delamination, which affects laminated composites. Because of the improved mechanical behavior, these materials are increasingly used in a variety of engineering applications.[2] Developments of the processing techniques of FGMs are constantly made,[3] and the development of three-dimensional (3D) printing, which has the capability of extruding two different filaments from one nozzle,[4] will further increase FGM usability.

Cracking and fracture of such materials can occur and have been extensively investigated, as described in the literature.[5–8] Numerical models, such as integral equations,[7–12] boundary elements,[13,14] and the finite element method,[15–20] have been used to investigate FGMs. A comprehensive review of the various analytical and numerical methods employed to study the static, dynamic, and stability behaviors of FGM plates is given in Swaminathan et al.[21] All possible evaluation techniques of such materials (aimed at enriching numerical capability) should be investigated. Having more than one numerical technique that converges to the same result, especially in problems that do not have analytical solutions, is an advantage.

In this investigation, the finite difference (FD) method is applied to solve crack problems in FGMs. The accuracy that can be achieved in the calculation of stress intensity factors (SIFs) is checked for a mode I crack problem in FGMs. This technique is simple and easy to apply. It was successfully applied to investigate 3D delamination,[22] and bimaterial crack problems with contact and friction

Faculty of Mechanical Engineering, Technion – Israel Institute of Technology, Haifa, Israel

Corresponding author:
A Dorogoy, Faculty of Mechanical Engineering, Technion – Israel Institute of Technology, 32000 Haifa, Israel.
Email: dorogoy@technion.ac.il

between the crack faces of linear *homogeneous* elastic materials.[23–25]

Three post-processing routines for SIF determination were implemented. In Section 2, the linear elastic two-dimensional formulation for FGMs is presented. The equilibrium equations and the boundary conditions are transformed to an orthogonal curvilinear coordinate system and written explicitly. A verification of the technique is performed in Section 3, wherein two test cases with analytical solutions are solved successfully.[26] Section 4 addresses the edge crack problem. The first part of this section details the three methods used to extract the SIF and their application in the FD technique. Then, the edge crack problem is introduced and solved. The manuscript ends with a summary and conclusions.

2. The FD formulation

The two-dimensional displacement equilibrium equations in an *x, y* Cartesian coordinate system for linear elastic FGMs with small strains, neglecting body forces, are given by:

$$(1+\mathrm{K})U,_{xx} + U,_{yy} + \mathrm{K}V,_{xy} + \frac{a,_x}{G}U,_x + \frac{b,_x}{G}V,_y + \frac{G,_y}{G}\left(U,_y + V,_x\right) = 0 \quad (1)$$

$$(1+\mathrm{K})V,_{yy} + V,_{xx} + \mathrm{K}U,_{xy} + \frac{a,_y}{G}V,_y + \frac{b,_y}{G}U,_x + \frac{G,_x}{G}\left(U,_y + V,_x\right) = 0 \quad (2)$$

where a comma represents differentiation. The last four terms in Equations (1) and (2), which include first derivative of the displacements, do not appear for homogeneous materials.[23–25] The material coefficients for the plane stress and plane strain conditions are detailed in Table 1. Young's modulus E and Poisson's ratio ν are functions of location: $E = f_1(x,y)$ and $\nu = f_2(x,y)$.

Stresses are related to displacements through Hooke's law as follows:

$$\sigma_{xx} = a\varepsilon_{xx} + b\varepsilon_{yy} = aU,_x + bV,_y \quad (3)$$

$$\sigma_{yy} = a\varepsilon_{yy} + b\varepsilon_{xx} = aV,_y + bU,_x \quad (4)$$

$$\sigma_{xy} = 2G\varepsilon_{xy} = G\left(U,_y + V,_x\right) \quad (5)$$

For plane strain:

$$\sigma_{zz} = \nu\left(\sigma_{xx} + \sigma_{yy}\right) = b\left(U,_x + V,_y\right) \quad (6)$$

For generality, the derivatives in the above equations are transformed to a curvilinear coordinate system (ξ, η) by means of the chain rule.[22–25] Such a transformation enables solutions in any curvilinear coordinates, e.g., rectangular or cylindrical coordinates,[23,24] and increases the capability of refining the mesh at areas of stress concentration, as will be shown in subsequent research. Transformed equilibrium Equations (1) and (2) in the *x*- and *y*-directions, respectively, are given by:

$$\left(b_1^g + b_1^h\right)U,_\xi + \left(b_2^g + b_2^h\right)U,_\eta + b_3^h U,_{\xi\xi} + b_4^h U,_{\eta\eta} + b_5^h U,_{\xi\eta} + \left(c_1^g + c_1^h\right)V,_\xi + \left(c_2^g + c_2^h\right)V,_\eta + c_3^h V,_{\xi\xi} + c_4^h V,_{\eta\eta} + c_5^h V,_{\xi\eta} = 0 \quad (7)$$

$$\left(d_1^g + d_1^h\right)V,_\xi + \left(d_2^g + d_2^h\right)V,_\eta + d_3^h V,_{\xi\xi} + d_4^h V,_{\eta\eta} + d_5^h V,_{\xi\eta} + \left(e_1^g + c_1^h\right)U,_\xi + \left(e_2^g + c_2^h\right)U,_\eta + c_3^h U,_{\xi\xi} + c_4^h U,_{\eta\eta} + c_5^h U,_{\xi\eta} = 0 \quad (8)$$

Coefficients $b_i^h,\ c_i^h,\ d_i^h\ i = 1\cdots5$ and $b_i^g, c_i^g,\ d_i^g,\ e_i^g\ i = 1\cdots2$ depend on material properties and mixed derivatives of both coordinates systems at an interior point of the FD mesh at which the equilibrium equations are imposed. Equations (7) and (8) are the same equations as those for homogeneous materials.[23–25] The only difference from the homogeneous case lies in coefficients $b_i^g,\ c_i^g,\ d_i^g, e_i^g\ i = 1\cdots2$. These coefficients appear because of the contribution of the four terms with a first derivative of the displacements in equilibrium Equations (1) and (2). These terms appear because the material is nonhomogeneous. Coefficients $b_i^h,\ c_i^h,\ d_i^h\ i = 1\cdots5$ and $b_i^g,\ c_i^g, d_i^g, e_i^g\ i = 1\cdots2$ are detailed in Appendix A.

The stresses corresponding to Equations (3)–(6) are transformed to a curvilinear coordinate system via:

$$\sigma_{\xi\xi} = c_{11}U,_\xi + c_{12}U,_\eta + c_{13}V,_\xi + c_{14}V,_\eta \quad (9)$$

$$\sigma_{\eta\eta} = c_{21}U,_\xi + c_{22}U,_\eta + c_{23}V,_\xi + c_{24}V,_\eta \quad (10)$$

$$\sigma_{\xi\eta} = c_{31}U,_\xi + c_{32}U,_\eta + c_{33}V,_\xi + c_{34}V,_\eta \quad (11)$$

Coefficients $c_{ij},\ i = 1\cdots3,\ j = 1\cdots4$ depend on the mixed derivatives of both coordinate systems at the point of application of the boundary conditions, are given explicitly in Appendix A.

The tractions on the curvilinear boundary are given by:

$$T_i = \sigma_{ij}n_j \quad ; \quad i = \xi, \eta \quad ; \quad j = \xi, \eta \quad (12)$$

Table 1. Material coefficients.

Plane stress	Plane strain
$a = \frac{E}{1-\nu^2}$	$a = \frac{E(1-\nu)}{(1-2\nu)(1+\nu)}$
$b = \nu a = \frac{\nu E}{1-\nu^2}$	$b = \frac{E\nu}{(1-2\nu)(1+\nu)}$
$\mathrm{K} = \frac{1+\nu}{1-\nu}$	$\mathrm{K} = \frac{1}{1-2\nu}$
$G = \frac{E}{2(1+\nu)}$	

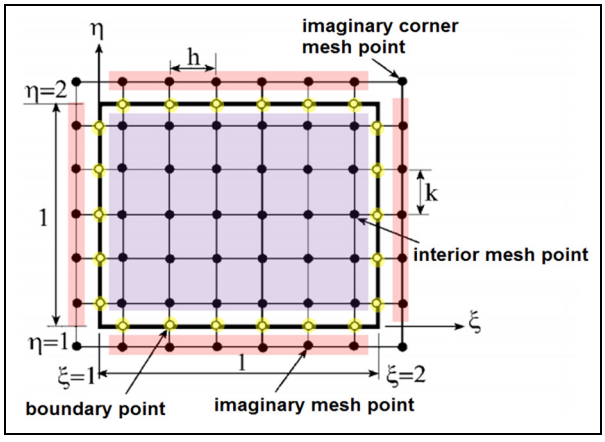

Figure 1. Finite difference mesh in the numerical domain.

where T_i are the tractions, σ_{ij} are the stresses in Equations (9)–(12), and n_j are the components of the outward unit normal to the boundary in the (ξ, η)directions. The displacements on the curvilinear boundary are given by:

$$U = c_{41}U_\xi + c_{42}U_\eta \tag{13}$$

$$V = c_{51}U_\xi + c_{52}U_\eta \tag{14}$$

where U_ξ and U_η are displacements in the curvilinear directions. Coefficients $c_{ij}\ ;\ i = 4\cdots5\ ;\ j = 1\cdots2$ are also presented in Appendix A.

The physical domain (x, y) is mapped into a Cartesian numerical domain (ξ, η)[23–25] in which $1 \leqslant \xi \leqslant 2$ and $1 \leqslant \eta \leqslant 2$, as shown in Figure 1. Equations (7)–(14) are used in the numerical domain. Mapping is performed using polynomial transformations given by[23]:

$$x = \sum_{i=0}^{M} s_i \xi^i \tag{15}$$

$$y = \sum_{i=0}^{N} t_i \eta^i \tag{16}$$

where $s_i\ ;\ i = 0\cdots M$ and $t_i\ ;\ i = 0\cdots N$ are constants. Proper choice of the coefficients allows for mesh refinement at the crack tip in the physical domain. The FD mesh in the numerical domain has a constant mesh size h and k in the ξ and η directions, respectively. The application of the FD technique is the same as in previous studies.[23–25]

Central FD formulas (stencils), as detailed in Appendix B, are substituted into Equations (7)–(11). The residuals of all the difference equations approach zero as $h^2 \rightarrow 0$ and $k^2 \rightarrow 0$.[23] At each mesh point, there are two unknowns, that is, displacements U and V. For each mesh point in the interior, there are two equilibrium equations (Equations (7) and (8)). For each imaginary mesh point, there are two boundary conditions applied on the adjacent boundary point (yellow). These boundary condition can be displacements, tractions or mixed traction-displacements. The values of the four imaginary corner mesh points are determined via linear extrapolation. The algebraic linear system of equations resulting from the substitution of the stencils into Equations (7)–(14) is programmed in Fortran 90 (Intel Fortran compiler, Intel Parallel Studio XE 2013, Intel Corporation) and solved with a Fortran library subroutine, Y12MAF (http://www.netlib.org/y12m/doc) that solves sparse systems of algebraic linear equations by Gaussian elimination.

3. Verification of the FD solution

Four test problems were solved to verify the accuracy of the FD technique. These test cases include material gradation but not stress concentration or stress singularities. The four simple test problems are described in Cartesian coordinates and have closed-form solutions for plane stress non-homogeneous isotropic materials.[26] The problems consist of uniaxial tension T in the x direction of a square plate with $0 \leqslant x \leqslant 1$ and $0 \leqslant y \leqslant 1$ and nonhomogeneous properties $E(x, y)$. In the first two problems, Young's modulus varies only along the x direction as $E(x) = \frac{E_0}{1 + \widehat{k}x}$ with $\widehat{k} = -0.5,\ 5$. The analytical solution for the displacements is found to be as follows[26]:

$$u_A(x,y) = \frac{T}{E_0}\left(x + \widehat{k}\left(\frac{x^2}{2} + \nu\frac{y^2}{2}\right)\right) \tag{17}$$

$$v_A(x,y) = -\nu\frac{T}{E_0}\left(1 + \widehat{k}x\right)y \tag{18}$$

In the third and fourth problems, Young's modulus varies only along the y direction as $E(y) = \frac{E_0}{1 + \widehat{k}y}$ with $\widehat{k} = -0.5,\ 5$. The analytical solution for the displacement is also found in Sadd[26]:

$$u_A(x,y) = \frac{T}{E_0}\left(1 + \widehat{k}y\right)x \tag{19}$$

$$v_A(x,y) = -\nu\frac{T}{E_0}\left(y + \widehat{k}\left(\frac{y^2}{2} + \frac{x^2}{2\nu}\right)\right) \tag{20}$$

The geometry, load, and a color map that shows the x distribution of $E(x)$ for $k = -0.5$ are shown in Figure 2(a). The variations of E along x for $\widehat{k} = -0.5$ and 5 are shown in Figure 2(b). In the numerical analyses, $E_0 = 1$, $\nu = 0.3$, and plane stress conditions prevail.

The boundary conditions applied numerically for all test cases are:

At $x = 0$: $T_x(0,y) = -\sigma_{xx}(0,y) = -1, T_y(0,y) = \sigma_{xy}(0,y) = 0$
At $x = 1$: $T_x(0,y) = \sigma_{xx}(1,y) = 1, \quad T_y(1,y) = \sigma_{xy}(0,y) = 0$
At $y = 0$: $u(x,0) = u_A(x,0)$ and $v(x,0) = v_A(x,0)$, where u_A and v_A are detailed in Equations (17)–(20).

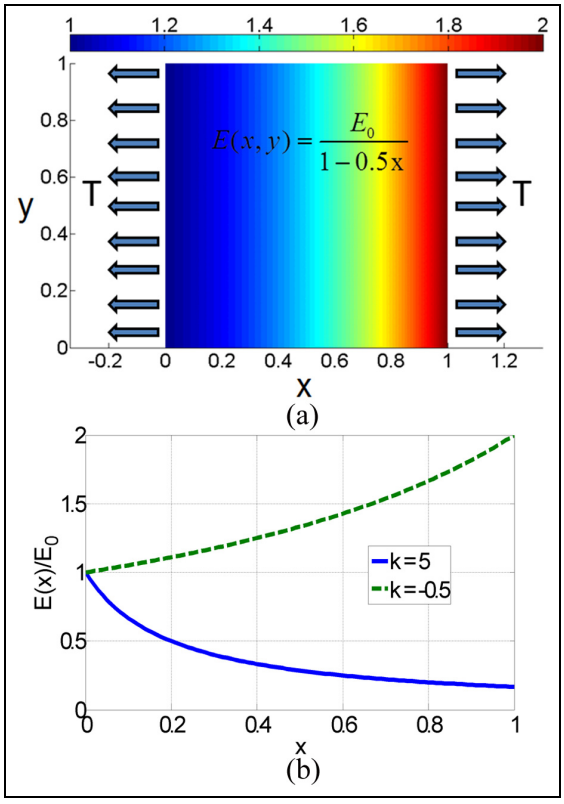

Figure 2. (a) Uniaxial tension on a thin (plane stress) square plate with a non-homogeneous E distribution. (b) The two distributions of $E(x)$ that were considered.

At y = 1: $T_x(x,1) = \sigma_{xy}(x,1) = 0$ and $T_y(x,1) = \sigma_{yy}(x,1) = 0$

3.1. Test case 1: material gradation along x with $\hat{k} = -0.5$ and $\hat{k} = 5$

An equal mesh size was used with application of linear transformations (Equations (15) and (16)), where $x = -1 + \xi$ and $y = -1 + \eta$. The mesh size was increased gradually until very good agreement between the numerical and analytical displacements of the upper free face at $y = 1$ was obtained. The initial number of mesh points was 20 × 20 and the final number was 150 × 150 points. These numbers correspond to mesh sizes in the transformed coordinates (ξ, η) of $h = k = 1/18 = 0.0556$ and $h = k = 1/148 = 0.0068$, respectively.

Figure 3(a) shows displacements u and v on the upper free face ($y = 1$) for the case where $\hat{k} = -0.5$ and compares analytical results u_A and v_A to numerical results u_n and v_n, which were obtained with a 20 × 20 coarse mesh and a 120 × 120 fine mesh. Even for the coarse mesh, results v_n are quite accurate, but results u_n need improvement. For the 120 × 120 fine mesh, very good agreement can be observed.

Figure 3(b) shows displacements u and v on the upper free face ($y = 1$) for the case where $\hat{k} = 5$. The results of u_n and v_n (obtained with a 20 × 20 coarse mesh and a 150 × 150 fine mesh, respectively) are presented along with the analytical displacements. For the coarse mesh, results for v_n differ significantly from the analytical results, while results for u_n are quite accurate. For the fine mesh (150 × 150), very good agreement can be observed.

The relative error of the displacements is calculated via:

$$error_u\,[\%] = 100\,\frac{u_n(x_i) - u_A(x_i)}{u_A^{\max}} \tag{21}$$

$$error_v\,[\%] = 100\,\frac{v_n(x_i) - v_A(x_i)}{u_A^{\max}} \tag{22}$$

where x_i is a mesh point along the boundary and $u_A^{\max}$ is the maximum displacement u at $(x, y) = (1, 1)$. The errors for the case where $\hat{k} = -0.5$ indicate that, for the coarse mesh, the error in u_n is less than 7% (except from the corner point at $(x, y) = (0, 1)$). For the fine mesh, the maximum error drops below 1.1%.

The results for the case where $\hat{k} = 5$ indicate that the usage of the 20 × 20 coarse mesh results in considerably large errors; the error of u_n reaches 15% and the error of v_n reaches 5%. Increasing the number of mesh points to 120 × 120 reduces the errors significantly. The maximum error in u_n is 2.7%, while the errors in v_n are all below 1%. A further increase of the number of points to 150 × 150 reduces the maximum error in u_n to 2.2%, while the errors of v_n remain below 1%.

3.2. Test case 2: material gradation along y with $\hat{k} = -0.5$ and $\hat{k} = 5.0$

An equal size coarse mesh of 20 × 20 points was used to solve this problem. The results of the coarse mesh were verified by using a finer mesh of 40 × 40 points. The accuracy of the displacements on the upper free face at $y = 1$ was checked with the aid of Equations (21) and (22). Figure 4 shows the analytical displacements on the upper face alongside the numerical ones. Figure 4(a) shows the case where $\hat{k} = -0.5$ and Figure 4(b) shows the case where $\hat{k} = 5.0$. Excellent agreement can be observed for both cases (even for the coarse mesh). The error is less than 0.01% (except from the corner point at $(x, y) = (0, 1)$, at which it is 3%). The finer mesh with 40 × 40 points confirms the results obtained by the coarse mesh.

3.3. Summary

The results of these test cases verify the accuracy of the FD method presented. The results demonstrate convergence, that is, the smaller the mesh size, the more accurate the results. A considerably fine mesh is needed to obtain

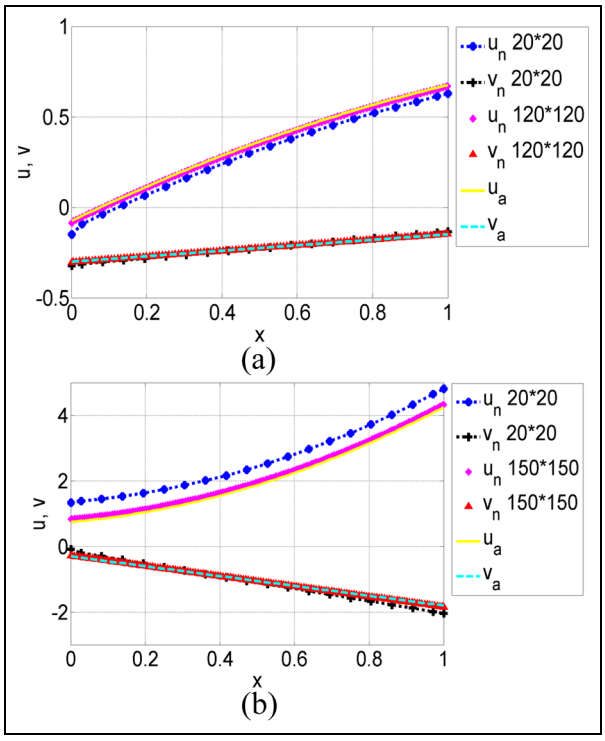

Figure 3. Comparison between analytical and numerical results of the displacements at $y = 1$. The material is graded in the x direction. (a) $\widehat{k} = -0.5$. (b) $\widehat{k} = 5$.

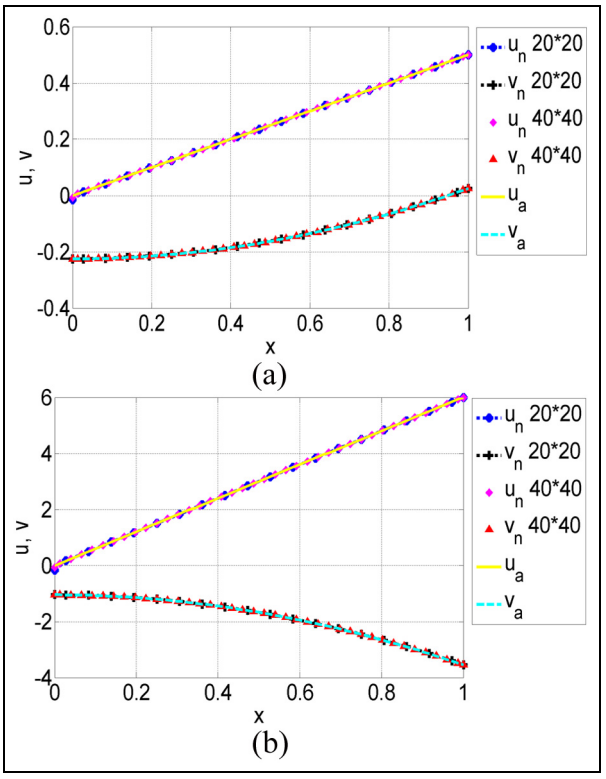

Figure 4. Comparison between analytic and numerical results of the displacements at $y = 1$. The material is graded in the y direction. (a) $\widehat{k} = -0.5$. (b) $\widehat{k} = 5$.

accurate results when the direction of the material gradation and the load coincide (test cases 1 and 2). A coarse mesh is needed when the material gradation and the load direction do not coincide (test cases 3 and 4). A crack problem with *stress singularity* will be examined next.

4. The edge crack problem

The aim of this section is to demonstrate the application of the FD technique for solving crack problems in FGMs. An edge crack is a common type of structural damage, and therefore, it is very useful to investigate its fracture characteristics. Many studies have investigated the mode I SIFs of cracks in FGMs in unbounded materials.[9,11,12] Erdogan and Wu solved an edge problem in a bounded region composed of a long strip of finite width in an FGM material.[10] They assumed that the shear modulus is graded exponentially along the width, and the Poisson's ratio remains constant. The purpose of this investigation is to first reproduce the results obtained by Erdogan and Wu,[10] using the FD method.

The methods used to extract the mode I SIF from the FD results are summarized and explained, and then the problem and results are introduced.

4.1. Methods for calculating the mode I SIF

Three methods have been used in this investigation to extract the mode I SIF from the FD results. They all involve the J integral.[27] These methods have been applied in other investigations for finite elements results.[16,17,19,20] They are briefly introduced here and their application for FD results is explained.

4.1.1. A path-dependent J line. The line integral J is as follows[27]:

$$J_0 = \int_{\Gamma_0} \left(W n_x - T_i \frac{\partial u_i}{\partial x} \right) d\Gamma \tag{23}$$

where path Γ_0 is *any* path that starts on the bottom crack face, surrounds the crack tip counterclockwise and ends on the upper crack face. An example of such a path is shown in Figure 5(a). The displacements are u_i, the tractions along this path are $T_i = \sigma_{ij} n_j$ and n_j are the components of the outward normal to the path. The strain energy density is given by $W = \frac{1}{2}\sigma_{ij}\varepsilon_{ij}$. A circular path for computing J line Γ_ε, which surrounds the crack tip at $r = \varepsilon$, is also shown schematically in Figure 5(a). The value of this integral when $\varepsilon \to 0$ is J_ε.

Eischen[5] has shown that for FGMs:

$$J_\varepsilon = \int_{\Gamma_\varepsilon} \left(W n_x - T_i \frac{\partial u_i}{\partial x} \right) d\Gamma = \frac{K_I^2 + K_{II}^2}{E'_{tip}} \tag{24}$$

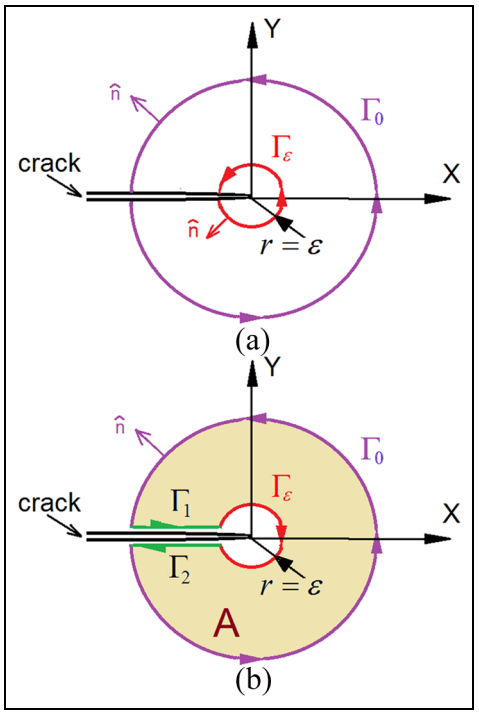

Figure 5. A schematic crack tip in FGM material. (a) Paths Γ_0 and Γ_ε used to calculate the *J* integral. (b) A closed path used to calculate the *J* line. The path surrounds area *A* and excludes the crack tip.

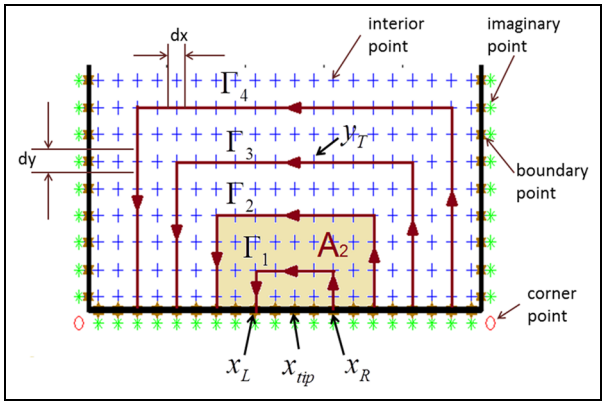

Figure 6. A typical FD mesh on a symmetric cracked component (upper half only) with four typical paths for calculating the J line. The crack tip is located at x_{tip}.

where

$$\begin{cases} E_{tip} = E_{tip} & plane\ \ stress \\ E = \frac{E_{tip}}{1-\nu_{tip}^2} & plane\ \ strain \end{cases} \tag{25}$$

The subscript "tip" denotes the values at (x_{tip}, y_{tip})—the coordinates of the crack tip. Once J_ε is known, the mode I SIF can be calculated by:

$$K_I = \sqrt{J_\varepsilon E'} \tag{26}$$

A typical rectangular FD mesh on a cracked component is shown in Figure 6. The crack tip lies at $(x, y) = (x_{tip}, 0)$. Because of symmetry, only the region above the crack is considered. Four typical lines for calculating J are also illustrated. The path starts at $(x_R, 0)$, climbs vertically to (x_R, y_T), continues horizontally to (x_L, y_T) and ends on the crack face at $(x_L, 0)$. Integrand ΔJ_i of Equation (24) is calculated by summing each interior point i that lies on the path to approximate the integral as $J_0 \cong \sum_i \Delta J_i \, d\Gamma_i$, where $d\Gamma_i = dx_i$ or $d\Gamma_i = dy_i$.

Integration is performed symmetrically on both sides of the crack tip, that is, $|x_{tip} - x_R| = |x_{tip} - x_L|$, and when $|x_{tip} - x_R| \equiv \rho \to 0$, the area encircled by the path approaches zero and the value of J corresponds to J_ε. The integral is calculated over many paths and the results are curve-fitted by polynomial $J_0 \cong f(\rho)$. Here J_ε is calculated by taking the limit $\lim_{\rho \to 0}[f(\rho)]$.

4.1.2. A conservative J integral. A closed path for calculating the J line is shown in Figure 5(b). The path surrounds area A and excludes the crack tip. The value of the J integral can be written as:

$$J_0 - J_\varepsilon = \oint_{\Gamma_0 + \Gamma_1 + \Gamma_2 + \Gamma_\varepsilon} \left(W n_x - T_i \frac{\partial u_i}{\partial x} \right) d\Gamma \tag{27}$$

Note that along crack faces Γ_1 and Γ_2, the integrand vanishes, and along Γ_ε, normal $\hat{n}$ points inward. By invoking the divergence theorem, Equation (27) can be written as:

$$J_0 - J_\varepsilon = \int_A \left[\frac{\partial W}{\partial x} - \frac{\partial}{\partial x_j} \left(\sigma_{ij} \frac{\partial u_i}{\partial x} \right) \right] dA \tag{28}$$

The derivative of the strain energy is as follows:

$$\frac{\partial W}{\partial x} = \frac{\partial W}{\partial \varepsilon_{ij}} \frac{\partial \varepsilon_{ij}}{\partial x} + \frac{\partial W}{\partial E} \frac{\partial E}{\partial x} + \frac{\partial W}{\partial \nu} \frac{\partial \nu}{\partial x} = \sigma_{ij} \frac{\partial \varepsilon_{ij}}{\partial x} + \frac{\partial W}{\partial E} \frac{\partial E}{\partial x} + \frac{\partial W}{\partial \nu} \frac{\partial \nu}{\partial x} \tag{29}$$

For homogeneous materials where $\frac{\partial E}{\partial x} = \frac{\partial \nu}{\partial x} = 0$, the integral of Equation (28) equals 0 and $J_0 - J_\varepsilon = 0$; therefore, $J_0 = J_\varepsilon$ and J integral is path independent.

For FGMs, it becomes as follows:

$$J_0 - J_\varepsilon = \int_A \left[\frac{\partial W}{\partial E} \frac{\partial E}{\partial x} + \frac{\partial W}{\partial \nu} \frac{\partial \nu}{\partial x} \right] dA \equiv \int_A \frac{\partial W^*}{\partial x} dA \tag{30}$$

Therefore:

$$J_\varepsilon = J_0 - \int_A \frac{\partial W^*}{\partial x} dA \tag{31}$$

Equation (31) is path independent but includes both line integral J_0 and an area integral. The calculation of J_0 is performed as explained in Section 4.1.1. The area encircled by path Γ_2 is shown in Figure 6. The integrand in Equation (31) is calculated within each interior point i and summed as $\int_A \frac{\partial W^*}{\partial x} dA \cong \sum_i \left(\frac{\partial W^*}{\partial x}\right)_i dA_i$, where $dA_i = dx_i dy_i$ is the area associated with internal mesh point *i*.

4.1.3. A conservative J area integral. If we have a continuous function q with values of zero along Γ_0 and 1 along Γ_ε, we can multiply both sides of Equation (28) to get the following:

$$(J_0 - J_\varepsilon)q = -J_\varepsilon = \oint_{\Gamma_0 + \Gamma_1 + \Gamma_2 + \Gamma_\varepsilon} \left(W n_x - T_i \frac{\partial u_i}{\partial x}\right) q d\Gamma \tag{32}$$

Invoking the divergence theorem on the right side of Equation (32):

$$-J_\varepsilon = \left[\int_A (W\delta_{jx} - T_i \frac{\partial u_i}{\partial x})\frac{\partial q}{\partial x_j} + [\frac{\partial W}{\partial x} - \frac{\partial}{\partial x_j}\left(\sigma_{ij}\frac{\partial u_i}{\partial x}\right)]\, q\right] dA \tag{33}$$

After some algebraic manipulation, the integral may be written as:

$$J_\varepsilon = \int_A (\sigma_{ij}\frac{\partial u_i}{\partial x} - W\delta_{jx})\frac{\partial q}{\partial x_j} dA - \int_A \frac{\partial W^*}{\partial x} q\, dA \tag{34}$$

The implementation of the area integral is the same as explained in Section 4.1.2.

Function q was chosen as:

$$q(x,y) = \frac{(x - x_L)(x - x_R)(y - y_T)}{(x_{tip} - x_L)(x_{tip} - x_R)(y_{tip} - y_T)} \tag{35}$$

The shape of q for $(x_{tip}, y_{tip}) = (0.5,\ 0.0)$ and $x_L = 0.2$, $x_R = 0.8$ and $y_T = 0.3$ is shown in Figure 7. Figure 7(a) shows a 3D image of q, and Figure 7(b) shows a color contour map. It is clearly observed that q has values of zero for Γ_0 and 1 for Γ_ε (crack tip).

4.2. The edge crack problem

Figure 8 shows the geometry of the edge crack problem. The height is eight times the width $\left(\frac{H}{W} = 4\right)$ to mimic a long strip, and length a of the crack is half width W $\left(\frac{a}{W} = 0.5\right)$. Two loading conditions were analyzed: tension and bending. The applied boundary conditions are:

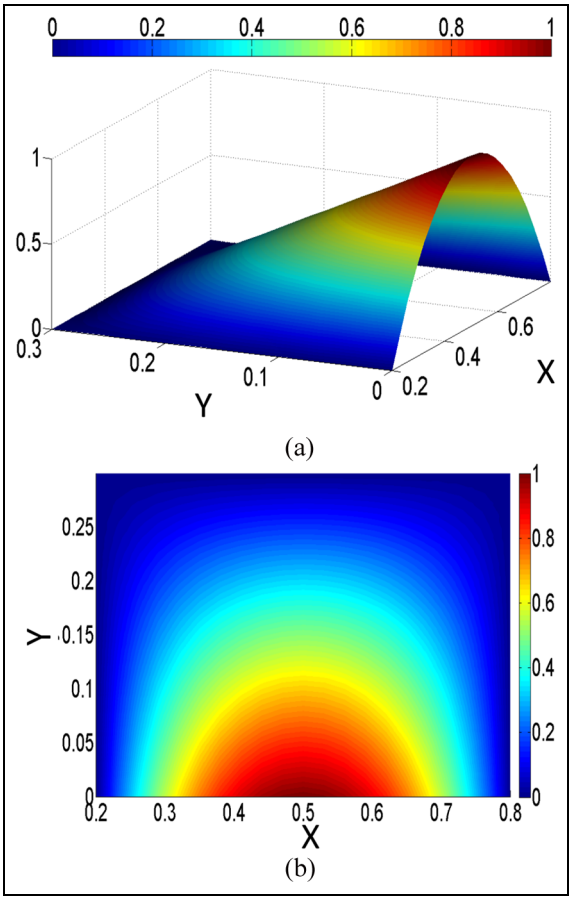

Figure 7. The shape of *q* used to calculate *J* area. (a) 3D view. (b) Color contour map.

$$T_y(x,H) = -T_y(x,-H) = \sigma_0 \qquad \textit{tension}$$

$$T_y(x,H) = -T_y(x,-H) = \sigma_0\left(1 - \frac{2x}{W}\right) \qquad \textit{bending}$$

The Young's modulus of an FGM is assumed to vary exponentially as $E(x) = E_1 e^{\beta x}$, and the Poisson's ratio is constant. Modulus variation $E(x)$ is characterized by two parameters: $E_1 = E(0)$ and $E_2 = E(W)$. Parameter $\beta = \frac{1}{W}\log\left(\frac{E_2}{E_1}\right)$. Plane strain conditions are assumed.

Because of symmetry, only the upper half is analyzed numerically. Free-face conditions $(\sigma_{yy} = \sigma_{xy} = 0)$ are applied for the crack face. The component is fixed in space by constraining the crack tip: $u = v = 0$. Symmetry conditions $v = 0$, $\frac{\partial u}{\partial y} = 0$ are applied all along the symmetry line.

In the analyses, the following parameters were used: $W = 1$, $a = 0.5$, $H = 4$, $E_1 = 1000$, $\upsilon = 0.3$, and $\sigma_0 = 10$. A non-uniform mesh, which is dense at the region of the crack tip, is used. A mesh with 160 mesh points in the x direction and 120 mesh points in the y direction is used. Figure 9 shows a transformation from the physical domain

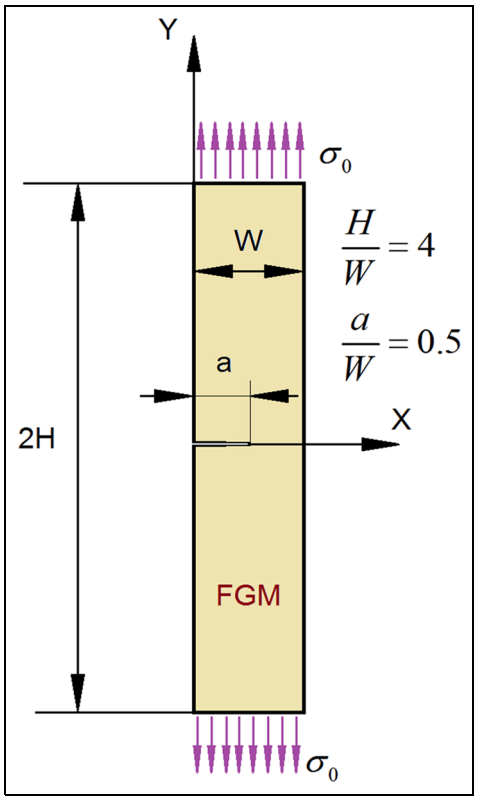

Figure 8. A long sheet with an edge crack.

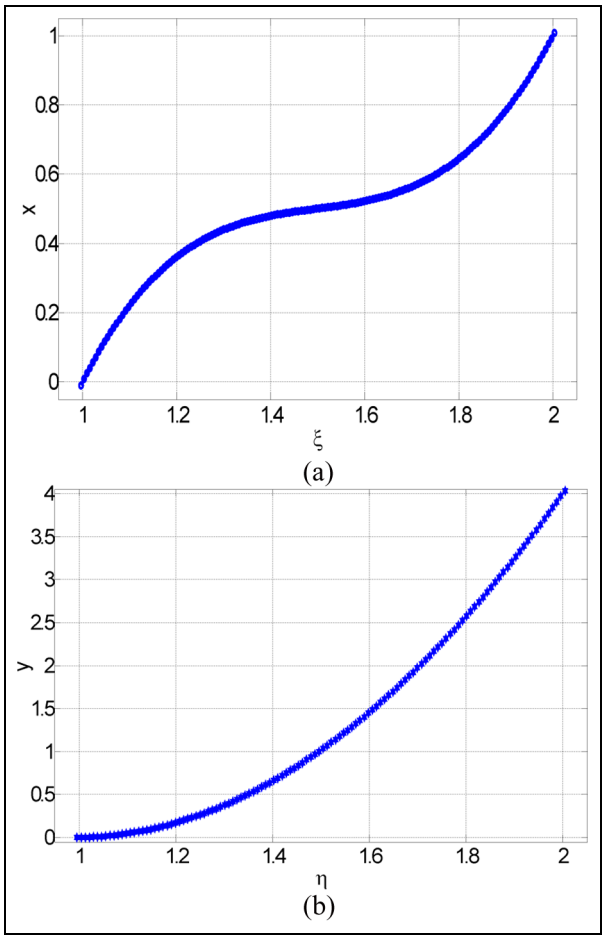

Figure 9. Transformation of physical region (x, y) to computational region (ξ,η). (a) Transformation of x (Equation (15)). (b) Transformation of y (Equation (16)).

to the numerical domain (Equations (15) and (16)). The mesh is dense where the derivatives $\frac{\partial x}{\partial \xi}$ and $\frac{\partial y}{\partial \eta}$ are small.

The mesh in physical domain (x, y) in the neighborhood of the crack tip, which is located at $(x_0, y_0) = (0.5, 0)$, is shown in Figure 10. The mesh sizes near the crack tip, Δx and Δy, are shown in the figure. The size of Δx and Δy shown is ~0.11% the crack length. The first three nearest paths for calculating J are shown in the figure.

4.3. Edge crack results

The edge crack problem was solved for two loading conditions: tension and bending. The following cases were solved: $\frac{E_2}{E_1} = 0.1, 0.2, 0.5, 1, 2, 5,$ and 10.

First, an example of the SIF calculation under tension loading for case $\frac{E_2}{E_1} = 0.1$ is shown. Figure 11 shows the results of 75 J_0, J_ε, and J_ε^{area} calculations along 75 paths and the areas they enclosed. The first three paths are shown in Figure 10. The path are symmetric in the x directions, i.e., $x_R - x_{tip} \simeq x_{tip} - x_L$, which means that when $x_R - x_{tip} \to 0$, area A around the crack tip is enclosed by such path $A \to 0$.

It is clearly observed that J_0 is path dependent, but its value for $x_R - x_{tip} \to 0$ converges to the expected value. Here J_ε (Section 4.1.2) and $J_\varepsilon^{\text{area}}$ (Section 4.1.3) are path independent, and a constant value is obtained for J for any distance from the crack tip. Some small divergence is observed near the crack tip because FD does not accurately predict the field very close to the crack tip. J_0 is approximated by a fourth-order polynomial, from which the limit when $x_R - x_{tip} \to 0$ is extracted: $\frac{J_0}{\sigma_0 a}_{\varepsilon \to 0} = 1.195$. Averaging the values of J_ε and $J_\varepsilon^{\text{area}}$ in $0.2 < \frac{x_R - x_{tip}}{a} < 0.6$ yields the normalized values 1.1144 and 1.1196, respectively. Mode I SIF is calculated using Equations (25) and (26) as the following values (which are normalized by $\sigma_0\sqrt{\pi a}$): 3.636, 3.511, and 3.519 for J_0, J_ε, and $J_\varepsilon^{\text{area}}$, respectively.

Table 2 summarizes the results and compares them to the results obtained in (10) using $dif = \frac{K_I^* - K_I^{FD}}{K_I^*}$ [%], where K_I^* is the result obtained in Erdogan and Wu.[10] Tables 2 and 3 summarize the results for tensional loading and bending loading, respectively. The cases solved numerically are: $\frac{E_2}{E_1} = 0.1,$ 0.2, 0.5, 1, 2, 5, and 10. Very good agreement between the FD results and those of Erdogan

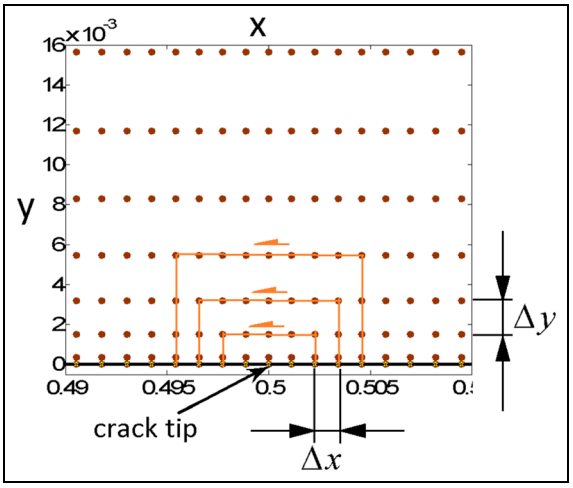

Figure 10. Mesh in (*x*, *y*) near the crack tip.

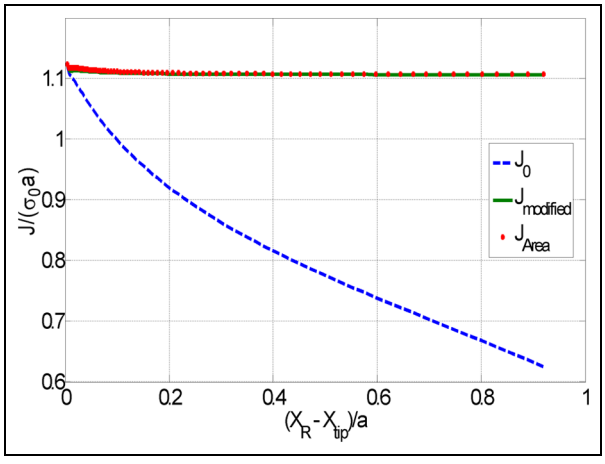

Figure 11. Results of calculations of J_0, J_ε, and J_ε^{area} versus the distance of the path from the crack tip.

and Wu,[10] the analytic results for $\frac{E_2}{E_1} = 1$ having been taken from Anderson,[28] can be observed in Tables 2 and 3; *differences are less than 1% except for three cases* (out of 16): $\frac{E_2}{E_1} = 0.1$ in tension loading, and $\frac{E_2}{E_1} = 0.1$ and 0.2 for bending loading. The maximum difference in tension is 1.97%. In bending loading, the maximum difference is 2.63%.

Overall, the good agreement with the results of Erdogan and Wu,[10] and the agreement between the three post-processors applied on the FD results, confirm the reliability to the FD method.

5. Summary and conclusions

A linear elastic two-dimensional formulation for FGMs in the (*x, y*) coordinate system is presented. The formulation of the equilibrium equations and boundary conditions were transformed into the orthogonal curvilinear coordinate system and were written explicitly. The FD technique was used to solve the above formulation using the Fortran 90 programming language. The solution technique was first verified by solving two test problems, in which the material was graded horizontally and vertically. A comparison with the analytical results showed very good agreement. The solution technique was then applied to solve an edge crack in a long layer. The Young's modulus of the layer was assumed to vary exponentially with width. The problem was solved for two loading conditions: tension and bending. To extract the mode I SIF from the FD results, three post-processor routines were developed and applied: (a) *J* line close to the crack tip, (b) a conservative *J* integral for FGM, and (c) a conservative *J* area integral for FGMs. All three methods provided similar results and were in excellent agreement with the semi-analytical results of

Table 2. Normalized stress intensity factors obtained by FD for tensional loading and their relative difference from Erdogan and Wu.[10] The analytic results for $\frac{E_2}{E_1} = 1$ are from Anderson.[28]

$\frac{E_2}{E_1}$		J_0	J_ε	J_ε^{area}	Erdogan and Wu[10]
0.1	$\frac{K_I}{\sigma_0\sqrt{\pi a}}$	3.5231	3.4999	3.5014	3.5701
	dif [%]	1.32	1.97	1.93	
0.2	$\frac{K_I}{\sigma_0\sqrt{\pi a}}$	3.3196	3.301	3.3023	3.3266
	dif [%]	0.21	0.77	0.73	
0.5	$\frac{K_I}{\sigma_0\sqrt{\pi a}}$	3.0401	3.0276	3.0288	3.0331
	dif [%]	0.23	0.18	0.14	
1	$\frac{K_I}{\sigma_0\sqrt{\pi a}}$	2.8286	2.8208	2.8217	2.8266
	dif [%]	0.07	0.21	0.17	
2	$\frac{K_I}{\sigma_0\sqrt{\pi a}}$	2.6213	2.6179	2.6187	2.6233
	dif [%]	0.08	0.21	0.18	
5	$\frac{K_I}{\sigma_0\sqrt{\pi a}}$	2.3576	2.3595	2.3601	2.3656
	dif [%]	0.37	0.26	0.23	
10	$\frac{K_I}{\sigma_0\sqrt{\pi a}}$	2.1679	2.173	2.1736	2.1762
	dif [%]	0.38	0.15	0.12	

Table 3. Normalized stress intensity factors obtained by FD for bending loading and their relative difference from Erdogan and Wu.[10] The analytic results for $\frac{E_2}{E_1} = 1$ are from Anderson.[28]

$\frac{E_2}{E_1}$		J_0	J_ε	$J_\varepsilon^{\text{area}}$	Erdogan and Wu[10]
0.1	$\frac{K_I}{\sigma_0\sqrt{\pi a}}$	2.168	2.1568	2.1579	2.2151
	$dif\ [\%]$	2.13	2.63	2.58	
0.2	$\frac{K_I}{\sigma_0\sqrt{\pi a}}$	1.9323	1.9232	1.9241	1.9534
	$dif\ [\%]$	1.08	1.55	1.50	
0.5	$\frac{K_I}{\sigma_0\sqrt{\pi a}}$	1.6649	1.6589	1.6596	1.6744
	$dif\ [\%]$	0.57	0.93	0.88	
1	$\frac{K_I}{\sigma_0\sqrt{\pi a}}$	1.4895	1.4859	1.4865	1.4752
	$dif\ [\%]$	-0.97	-0.73	-0.77	
2	$\frac{K_I}{\sigma_0\sqrt{\pi a}}$	1.3334	1.332	1.3325	1.3406
	$dif\ [\%]$	0.54	0.64	0.6042	
5	$\frac{K_I}{\sigma_0\sqrt{\pi a}}$	1.1518	1.153	1.1534	1.1518
	$dif\ [\%]$	0.0004	-0.10	-0.13	
10	$\frac{K_I}{\sigma_0\sqrt{\pi a}}$	1.0306	1.0333	1.0336	1.035
	$dif\ [\%]$	0.43	0.16	0.14	

Erdogan and Wu.[10] This agreement indicates that the obtained stress and strain fields are accurate, which also leads to accurate results for the J integrals. These results demonstrate the applicability of the FD technique for solving crack problems in FGMs. The accurate SIF results encourage further study in the field of fracture mechanics associated with contact and friction, as in previous studies.[23–25]

Acknowledgement

The assistance and support of Professor Daniel Rittel is greatly appreciated.

Funding

This research received no specific grant from any funding agency in the public, commercial, or not-for-profit sectors.

References

1. Sobczak JJ and Drenchev L. Metallic functionally graded materials: a specific class of advanced composites. *J Mater Sci Technol* 2013; 29: 297–316.
2. Jha DK, Kant T and Singh RK. A critical review of recent research on functionally graded plates. *Compos Struct* 2013; 96: 833–849.
3. Kieback B, Neubrand A and Riedel H. Processing techniques for functionally graded materials. *Mater Sci Eng A* 2003; 362: 81–106.
4. Garland A and Fadel G. Design and manufacturing functionally gradient material objects with an off the shelf three-dimensional printer: challenges and solutions. *J Mech Des* 2015; 137: 111407.
5. Eischen JW. Fracture of nonhomogeneous materials. *Int J Fract* 1987; 34: 3–22.
6. Erdogan F. Fracture mechanics of functionally graded materials. *Compos Eng* 1995; 5: 753–770.
7. Gu P and Asaro RJ. Crack deflection in functionally graded materials. *Int J Solids Struct* 1997; 34: 3085–3098.
8. Jin Z-H and Batra RC. Some basic fracture mechanics concepts in functionally graded materials. *J Mech Phys Solids* 1996; 44: 1221–1235.
9. Konda N and Erdogan F. The mixed mode crack problem in a nonhomogeneous elastic medium. *Eng Fract Mech* 1994; 47: 533–545.
10. Erdogan F and Wu BH. The surface crack problem for a plate with functionally graded properties. *J Appl Mech* 1997; 64: 449–456.
11. Ozturk M and Erdogan F. Mode I crack problem in an inhomogeneous orthotropic medium. *Int J Eng Sci* 1997; 35: 869–883.
12. Ozturk M and Erdogan F. The mixed mode crack problem in an inhomogeneous orthotropic medium. *Int J Fract* 1999; 98: 243–261.
13. Yue ZQ, Xiao HT and Tham LG. Boundary element analysis of crack problems in functionally graded materials. *Int J Solids Struct* 2003; 40: 3273–3291.
14. Paulino GH, Sutradhar A and Gruy LJ. Boundary element methods for functionally graded materials. *WIT Trans Modell Simul* 2003: 34.
15. Kim J-H and Paulino GH. Finite element evaluation of mixed mode stress intensity factors in functionally graded materials. *Int J Numer Methods Eng* 2002; 53: 1903–1935.
16. Kim J-H and Paulino GH. Isoparametric graded finite elements for nonhomogeneous isotropic and orthotropic materials. *J Appl Mech* 2002; 69: 502–514.
17. Anlas G, Santare MH and Lambros J. Numerical calculation of stress intensity factors in functionally graded materials. *Int J Fract* 2000; 104: 131–143.
18. Bhardwaj G, Singh IV, Mishra BK, et al. Numerical simulation of functionally graded cracked plates using NURBS

based XIGA under different loads and boundary conditions. *Compos Struct* 2015; 126: 347–359.
19. Chen J, Wu L and Du S. A modified J integral for functionally graded materials. *Mech Res Commun* 2000; 27: 301–306.
20. Gu P, Dao M and Asaro RJ. A simplified method for calculating the crack-tip field of functionally graded materials using the domain integral. *J Appl Mech* 1999; 66: 101–108.
21. Swaminathan K, Naveenkumar DT, Zenkour AM, et al. Stress, vibration and buckling analyses of FGM plates: a state-of-the-art review. *Compos Struct* 2015; 120: 10–31.
22. Altus E and Dorogoy A. A three-dimensional study of delamination. *Eng Fract Mech* 1989; 33: 1–19.
23. Dorogoy A and Banks-Sills L. Shear loaded interface crack under the influence of friction: a finite difference solution. *Int J Numer Methods Eng* 2004; 59: 1749–1780.
24. Dorogoy A and Banks-Sills L. Effect of crack face contact and friction on Brazilian disk specimens: a finite difference solution. *Eng Fract Mech* 2005; 72: 2758–2773.
25. Dorogoy A and Banks-Sills L. A rigid punch on an elastic half-space under the effect of friction: a finite difference solution. In: *ASME 2008 9th biennial conference on engineering systems design and analysis*, Haifa, 7–9 July 2008, pp. 259–271. New York: ASME.
26. Sadd MH. Some simple Cartesian solutions to plane nonhomogeneous elasticity problems. *Mech Res Commun* 2010; 37: 22–27.
27. Rice JR. A path independent integral and the approximate analysis of strain concentration by notches and cracks. *J Appl Mech* 1968; 35: 379–386.
28. Anderson TL. *Fracture mechanics*. Boca Raton, FL: CRC Press, 2017.

Appendix A

Coefficients for equilibrium equations and boundary conditions in the curvilinear orthogonal coordinate system

Let (ξ, η) be a curvilinear orthogonal coordinate system in which $x = X(\xi, \eta)$ and $y = Y(\xi, \eta)$. Let $f(x,y) = f[X(\xi,\eta), Y(\xi,\eta)]$ be any function on that two-dimensional region. Using the ''chain rule of derivatives,'' the first derivative can be written as:

$$f_{,i} = f_{,x}x_{,i} + f_{,y}y_{,i} \qquad i = \xi, \eta \tag{A1}$$

The second derivative is:

$$\begin{aligned} f_{,ij} = {} & f_{,xx}x_{,j}x_{,i} + f_{,xy}\left(y_{,j}x_{,i} + y_{,i}x_{,j}\right) \\ & + f_{,yy}y_{,j}y_{,i} + f_{,x}x_{,ij} + f_{,y}y_{,ij} \end{aligned} \tag{A2}$$

Here, $ij = (\xi\xi, \eta\eta, \xi\eta)$.

Solving the two equations (Equations (A1)) yields the following:

$$\begin{aligned} f_{,x} &= \frac{1}{J}\left(y_{,\eta}f_{,\xi} - y_{,\xi}f_{,\eta}\right) \\ f_{,y} &= \frac{1}{J}\left(-x_{,\eta}f_{,\xi} + x_{,\xi}f_{,\eta}\right) \end{aligned} \tag{A3}$$

where the Jacobian is:

$$J = x_{,\xi}y_{,\eta} - y_{,\xi}x_{,\eta} \tag{A4}$$

The solution of the three equations (Equation (A2)) can be written as:

$$\begin{Bmatrix} f_{,xx} \\ f_{,yy} \\ f_{,xy} \end{Bmatrix} = \begin{bmatrix} a_{xx} & b_{xx} & c_{xx} & d_{xx} & e_{xx} \\ a_{yy} & b_{yy} & c_{yy} & d_{yy} & e_{yy} \\ a_{xy} & b_{xy} & c_{xy} & d_{xy} & e_{xy} \end{bmatrix} \begin{Bmatrix} f_{,\xi} \\ f_{,\eta} \\ f_{,\xi\xi} \\ f_{,\eta\eta} \\ f_{,\xi\eta} \end{Bmatrix}, \tag{A5}$$

where coefficients a_{ij}, b_{ij}, and c_{ij} $(ij = xx, yy, xy)$ in Equation (A5) depend on both coordinate systems and are given explicitly below:

$$\begin{aligned} a_{xx} = \frac{1}{J^3}\Big(& -2y_{,\xi\eta}y_{,\eta}x_{,\eta}y_{,\xi} + 2x_{,\xi\eta}y_{,\xi}y_{,\eta}^2 + y_{,\eta\eta}x_{,\eta}y_{,\xi}^2 \\ & - x_{,\eta\eta}y_{,\eta}y_{,\xi}^2 + y_{,\xi\xi}y_{,\eta}^2x_{,\eta} - x_{,\xi\xi}y_{,\eta}^3\Big) \end{aligned} \tag{A6}$$

$$\begin{aligned} b_{xx} = \frac{1}{J^3}\Big(& 2y_{,\xi\eta}y_{,\xi}y_{,\eta}x_{,\xi} - 2x_{,\xi\eta}y_{,\xi}^2y_{,\eta} - y_{,\eta\eta}y_{,\xi}^2x_{,\xi} \\ & + x_{,\eta\eta}y_{,\xi}^3 - y_{,\xi\xi}y_{,\eta}^2x_{,\xi} + x_{,\xi\xi}y_{,\eta}^2y_{,\xi}\Big) \end{aligned} \tag{A7}$$

$$c_{xx} = \frac{y_{,\eta}^2}{J^2} \tag{A8}$$

$$d_{xx} = \frac{y_{,\xi}^2}{J^2} \tag{A9}$$

$$e_{xx} = \frac{-2y_{,\xi}y_{,\eta}}{J^2} \tag{A10}$$

$$\begin{aligned} a_{yy} = \frac{1}{J^3}\Big(& -2y_{,\xi\eta}x_{,\eta}^2x_{,\xi} + 2x_{,\xi\eta}y_{,\eta}x_{,\xi}x_{,\eta} + y_{,\eta\eta}x_{,\eta}x_{,\xi}^2 \\ & - x_{,\eta\eta}y_{,\eta}x_{,\xi}^2 + y_{,\xi\xi}x_{,\eta}^3 - x_{,\xi\xi}x_{,\eta}^2y_{,\eta}\Big) \end{aligned} \tag{A11}$$

$$\begin{aligned} b_{yy} = \frac{1}{J^3}\Big(& 2y_{,\xi\eta}x_{,\eta}x_{,\xi}^2 - 2x_{,\xi\eta}x_{,\eta}x_{,\xi}y_{,\xi} - y_{,\xi\xi}x_{,\eta}^2x_{,\xi} \\ & + x_{,\eta\eta}y_{,\xi}x_{,\xi}^2 - y_{,\eta\eta}x_{,\xi}^3 + x_{,\xi\xi}x_{,\eta}^2y_{,\xi}\Big) \end{aligned} \tag{A12}$$

$$c_{yy} = \frac{x_{,\eta}^2}{J^2} \tag{A13}$$

$$d_{yy} = \frac{x,_{\xi}^{2}}{J^2} \tag{A14}$$

$$e_{yy} = \frac{-2x,_{\xi}x,_{\eta}}{J^2} \tag{A15}$$

$$a_{xy} = \frac{1}{J^3}\left(y,_{\xi\eta}y,_{\eta}x,_{\eta}x,_{\xi} + y,_{\xi\eta}y,_{\xi}x,_{\eta}^{2} - x,_{\xi\eta}y,_{\eta}^{2}x,_{\xi} - x,_{\xi\eta}y,_{\xi}y,_{\eta}x,_{\eta} - y,_{\eta\eta}x,_{\eta}x,_{\xi}y,_{\xi} + x,_{\eta\eta}y,_{\eta}y,_{\xi}x,_{\xi} - y,_{\xi\xi}y,_{\eta}x,_{\eta}^{2} + x,_{\xi\xi}y,_{\eta}^{2}x,_{\eta}\right) \tag{A16}$$

$$b_{xy} = \frac{1}{J^3}\left(-y,_{\xi\eta}y,_{\eta}x,_{\xi}^{2} - y,_{\xi\eta}y,_{\xi}x,_{\eta}x,_{\xi} + x,_{\xi\eta}y,_{\eta}y,_{\xi}x,_{\xi} + x,_{\xi\eta}y,_{\xi}^{2}x,_{\eta} + y,_{\eta\eta}x,_{\xi}^{2}y,_{\xi} - x,_{\eta\eta}y,_{\xi}^{2}x,_{\xi} + y,_{\xi\xi}y,_{\eta}x,_{\eta}x,_{\xi} - x,_{\xi\xi}y,_{\eta}x,_{\eta}y,_{\xi}\right) \tag{A17}$$

$$c_{xy} = -\frac{y,_{\eta}x,_{\eta}}{J^2} \tag{A18}$$

$$d_{xy} = -\frac{y,_{\xi}x,_{\xi}}{J^2} \tag{A19}$$

$$e_{xy} = \frac{x,_{\xi}y,_{\eta} + x,_{\eta}y,_{\xi}}{J^2}. \tag{A20}$$

Substitution of Equations (A6)–(A20) in the equilibrium equations yields the coefficients of the equilibrium equations (Equations (7) and (8)). Here *a, b, k*, and *G* are material parameters detailed in Table 1:

$$b_1^g = \frac{a,_x}{G}\frac{y,_{\eta}}{J} - \frac{G,_y}{G}\frac{x,_{\eta}}{J} \tag{A21}$$

$$b_1^h = (1 + \mathrm{K})\, a_{xx} + a_{yy} \tag{A22}$$

$$b_2^g = -\frac{a,_x}{G}\frac{y,_{\xi}}{J} + \frac{G,_y}{G}\frac{x,_{\xi}}{J} \tag{A23}$$

$$b_2^h = (1 + \mathrm{K})\, b_{xx} + b_{yy} \tag{A24}$$

$$b_3^h = (1 + \mathrm{K})\, c_{xx} + c_{yy} \tag{A25}$$

$$b_4^h = (1 + \mathrm{K})\, d_{xx} + d_{yy} \tag{A26}$$

$$b_5^h = (1 + \mathrm{K})\, e_{xx} + e_{yy} \tag{A27}$$

$$c_1^g = -\frac{b,_x}{G}\frac{x,_{\eta}}{J} + \frac{G,_y}{G}\frac{y,_{\eta}}{J} \tag{A28}$$

$$c_1^h = \mathrm{K} a_{xy} \tag{A29}$$

$$c_2^g = \frac{b,_x}{G}\frac{x,_{\xi}}{J} - \frac{G,_y}{G}\frac{y,_{\xi}}{J} \tag{A30}$$

$$c_2^h = \mathrm{K} b_{xy} \tag{A31}$$

$$c_3^h = \mathrm{K} c_{xy} \tag{A32}$$

$$c_4^h = \mathrm{K} d_{xy} \tag{A33}$$

$$c_5^h = \mathrm{K} e_{xy} \tag{A34}$$

$$d_1^g = -\frac{a,_y}{G}\frac{x,_{\eta}}{J} + \frac{G,_x}{G}\frac{y,_{\eta}}{J} \tag{A35}$$

$$d_1^h = (1 + \mathrm{K})\, a_{yy} + a_{xx} \tag{A36}$$

$$d_2^g = \frac{a,_y}{G}\frac{x,_{\xi}}{J} - \frac{G,_x}{G}\frac{y,_{\xi}}{J} \tag{A37}$$

$$d_2^h = (1 + \mathrm{K})\, b_{yy} + b_{xx} \tag{A38}$$

$$d_3^h = (1 + \mathrm{K})\, c_{yy} + c_{xx} \tag{A39}$$

$$d_4^h = (1 + \mathrm{K})\, d_{yy} + d_{xx} \tag{A40}$$

$$d_5^h = (1 + \mathrm{K})\, e_{yy} + e_{xx} \tag{A41}$$

$$e_1^g = \frac{b,_y}{G}\frac{y,_{\eta}}{J} - \frac{G,_x}{G}\frac{x,_{\eta}}{J} \tag{A42}$$

$$e_2^g = -\frac{b,_y}{G}\frac{y,_{\xi}}{J} + \frac{G,_x}{G}\frac{x,_{\xi}}{J} \tag{A43}$$

The coefficients for Equations (9)–(11) for application of traction boundary condition are as follows:

$$c_{11} = \frac{a_1(1-\nu)\, h_{\xi}^2 x,_{\xi}}{(1+\nu)(1-2\nu)} E \tag{A44}$$

$$c_{12} = \frac{a_2 \nu\, h_{\eta}^2 x,_{\eta}}{(1+\nu)(1-2\nu)} E \tag{A45}$$

$$c_{13} = \frac{a_1(1-\nu)\, h_{\xi}^2 y,_{\xi}}{(1+\nu)(1-2\nu)} E \tag{A46}$$

$$c_{14} = \frac{a_2 \nu\, h_{\eta}^2 y,_{\eta}}{(1+\nu)(1-2\nu)} E \tag{A47}$$

$$c_{21} = \frac{a_2 \nu\, h_{\xi}^2 x,_{\eta}}{(1+\nu)(1-2\nu)} E \tag{A48}$$

$$c_{22} = \frac{a_1(1-\nu) h_{\eta}^2 x,_{\eta}}{(1+\nu)(1-2\nu)} E \tag{A49}$$

$$c_{23} = \frac{a_1(1-\nu)\, h_{\eta}^2 y,_{\eta}}{(1+\nu)(1-2\nu)} E \tag{A50}$$

$$c_{24} = \frac{a_2 \nu\, h_{\xi}^2 y,_{\xi}}{(1+\nu)(1-2\nu)} E \tag{A51}$$

$$c_{31} = h_{\xi} h_{\eta} x,_{\eta} G \tag{A52}$$

$$c_{32} = h_{\xi} h_{\eta} x,_{\xi} G \tag{A53}$$

$$c_{33} = h_{\xi} h_{\eta} y,_{\eta} G \tag{A54}$$

$$c_{34} = h_{\xi} h_{\eta} y,_{\xi} G \tag{A55}$$

where

$$h_{\xi} = \frac{1}{\sqrt{(x,_{\xi})^2 + (y,_{\xi})^2}} \tag{A56}$$

$$h_\eta = \frac{1}{\sqrt{\left(x,_\eta\right)^2 + \left(y,_\eta\right)^2}} \tag{A57}$$

For plane strain, $a_1 = a_2 = a_3 = 1$, and for plane stress, $a_1 = (1-2\nu)/(1-\nu)^2$, $a_2 = (1-2\nu)/(1-\nu)$ and $a_3 = 0$.

The coefficients in Equations (13) and (14) for application of the displacement boundary conditions are given by:

$$c_{41} = h_\xi x,_\xi \tag{A58}$$

$$c_{42} = h_\eta x,_\eta \tag{A59}$$

$$c_{51} = h_\xi y,_\xi \tag{A60}$$

$$c_{52} = h_\eta y,_\eta \tag{A61}$$

Appendix B

Central finite difference formulas

Interior points:

$$\begin{Bmatrix} U,_x \\ U,_y \\ U,_{xx} \\ U,_{yy} \\ U,_{xy} \end{Bmatrix} = \begin{Bmatrix} \frac{U(i+1,j)-U(i-1,j)}{2h} \\ \frac{U(i,j+1)-U(i,j-1)}{2k} \\ \frac{U(i-1,j)-2U(i,j)+U(i+1,j)}{h^2} \\ \frac{U(i,j+1)-2U(i,j)+U(i,j-1)}{k^2} \\ \frac{U(i+1,j+1)+U(i-1,j-1)-U(i+1,j-1)-U(i-1,j+1)}{4hk} \end{Bmatrix} \tag{B1}$$

Boundary points: $n_\xi = \pm 1$

$$\begin{Bmatrix} U,_\xi \\ U,_\eta \end{Bmatrix} = \begin{Bmatrix} n_\xi \frac{U(i,j)-U(i-n_\xi,j)}{h} \\ \frac{1}{2}\left[\frac{U(i,j+1)-U(i,j-1)}{2k} + \frac{U(i-n_\xi,j+1)-U(i-n_\xi,j-1)}{2k}\right] \end{Bmatrix} \tag{B2}$$

Boundary points: $n_\eta = \pm 1$

$$\begin{Bmatrix} U,_\xi \\ U,_\eta \end{Bmatrix} = \begin{Bmatrix} \frac{1}{2}\left[\frac{U(i+1,j)-U(i-1,j)}{2h} + \frac{U\left(i+1,j-n_\eta\right)-U\left(i-1,j-n_\eta\right)}{2h}\right] \\ n_\eta \frac{U(i,j)-U\left(i,j-n_\eta\right)}{k} \end{Bmatrix} \tag{B3}$$

Author biography

Avraham Dorogoy gained his BSc in Mechanical Engineering (Cum Laude) in 1982, and MSc in 1985 at Technion, Haifa, Israel. Avraham holds a PhD in Mechanical Engineering since 2002 from Tel Aviv University, Israel. Avraham returned to the Faculty of Mechanical Engineering. Technion, Haifa, Israel at 2003 and is currently a senior research engineer and a senior adjunct lecturer in ''fracture mechanics.''